Scaling of brittle failure: strength versus toughness

Laurent Brochard, Sabri Souguir, Karam Sab

Scaling of brittle failure: strength versus toughness

Laurent Brochard · Sabri Souguir · Karam Sab

Abstract We study the scaling of strength and toughness in function of temperature, loading rate and system size, to investigate the difference between tensile failure and fracture failure. Molecular simulation is used to estimate the failure of intact and cracked bodies while varying temperature, strain rate and system size over many orders of magnitude, making it possible to identify scaling laws. Two materials are considered: an idealized toy model, for which a scaling law can be derived analytically, and a realistic molecular model of graphene. The results show that strength and toughness follow very similar scalings with temperature and loading rate, but differ markedly regarding the scaling with system size. Strength scales with the number of atoms whereas toughness scales with the number of cracks. It means that intermediate situations of moderate stress concentrations (e.g., notch) can exhibit not obvious size scaling, in-between those of strength and toughness. Following a theoretical analysis of failure as a thermally activated process, we could rationalize the observed scaling and formulate a general rate-temperature-size equivalence. The scaling law of the toy model can be derived rigorously but is not representative of real materials because of a force discontinuity in the potential. A more representative scaling law, valid for graphene, is proposed with a different exponent.

Keywords strength · toughness · scaling law · graphene

PACS 62.20.-x

L. Brochard
Laboratoire Navier, UMR 8205, École des Ponts, IFSTTAR, CNRS, UPE
6 & 8 avenue Blaise Pascal, 77455 Marne-la-Vallée Champs-sur-Marne, France.
Tel.: +33 1 64 15 37 88
E-mail: laurent.brochard@enpc.fr

S. Souguir
Laboratoire Navier, UMR 8205, École des Ponts, IFSTTAR, CNRS, UPE
6 & 8 avenue Blaise Pascal, 77455 Marne-la-Vallée Champs-sur-Marne, France.

K. Sab
Laboratoire Navier, UMR 8205, École des Ponts, IFSTTAR, CNRS, UPE
6 & 8 avenue Blaise Pascal, 77455 Marne-la-Vallée Champs-sur-Marne, France.

1 Introduction

Understanding mechanical failure is essential for the reliability of structures. Yet, the modeling of failure initiation remains quite debated. Many initiation criteria have been proposed in the literature but no consensus exists (Brochard et al, 2016). The various theories aim at reconciling two well understood limit cases, namely tensile strength and fracture toughness. Tensile strength, which describes the failure of flawless materials, is captured by a stress criterion (failure surface). In contrast, fracture toughness, which describes the failure of cracked bodies, is captured by an energy released criterion (linear elastic fracture mechanics). But a general theory of failure must be able to handle intermediary situations, that is to combine stress and energy in a more general criterion. So far, initiation theories have been postulated; e.g., cohezive zone models (Dugdale, 1960), non-local approaches (Novozhilov, 1969) or finite fracture mechanics (Leguillon, 2002). But a rigorous approach, necessary to reach a consensus, requires to understand the elementary physics at the heart of mechanical failure.

The most elementary scale of mechanical failure is the scale of atoms and molecules where atomic bonds

break and crack surface is created. While the physical evolution of macroscopic systems is described by continuum thermodynamics, at the atomic scale, fluctuations become significant and need to be accounted for, which is the purpose of statistical physics. In particular a general theory of failure should be able to relate the failure stress to the temperature-induced fluctuations through general scaling laws. Such a theory, called kinetic theory of strength, was proposed initially by Zhurkov (see Regel' et al (1972) or Zhurkov (1984)). This theory captures how failure stress $\sigma_{failure}$ depends on both temperature T and loading time τ through a general scaling law that has been verified for a wide variety of materials : $\tau \propto \exp\left(\frac{\Delta E(\sigma_{failure})}{kT}\right)$, with $\Delta E\left(\sigma_{failure}\right) > 0$ the energy barrier to reach the transition state to failure. One can recognize in this law the Boltzmann factor characteristic of thermally activated processes. Confrontation with experiments shows that, for most materials, $\Delta E \approx E_0 - \gamma\sigma$, hence :

$$\frac{\sigma_{failure}}{\sigma_{failure}\left(0K\right)} = 1 - \frac{T}{T_{cr}}\ln\left(\frac{\tau}{\tau_{cr}}\right) \qquad (1)$$

with τ_{cr} and T_{cr} two constants with dimensions of time and temperature respectively that depend on the material. The derivation of Equation 1 assumes that failure is the consequence of the occurrence of a transition state (e.g., breaking of a bond) associated with an energy barrier ΔE and with no reverse process (e.g., reformation of the bond), which is valid in the limit of small temperatures ($\Delta E_{reverse} - \Delta E \gg kT$).

Interestingly, thermally activated scaling laws are not confined to brittle failure but is encountered in many other failure mechanisms, although the expression of energy barrier ΔE may vary from one mechanism to another leading to different exponents on $T\ln\left(\tau\right)$ in Eq. (1) : plasticity of metallic glasses (Argon, 1979; Johnson and Samwer, 2005; Schuh et al, 2007), dislocation nucleation in ductile crystals (Zhu et al, 2008), yield by bond rotation in carbon nanotube (Wei et al, 2003; Dumitrica et al, 2006). A particular case of interest here is fracture failure, which has been investigated theoretically in the framework of thermal activation by Petrov and Orlov (1975, 1976). A key consideration pointed out by Petrov and Orlov is the size effect. Indeed, many 'competing' transitions states can lead to failure. For instance, in a body with many identical micro-cracks, each micro-crack can be the source of a macro-crack, but only one does actually become a macro-crack. This points to a difference in the scaling between fracture toughness and tensile strength, since the presence of flaws concentrates the transition states in the vicinity of the flaws.

In the literature, scaling and size effects of failure have attracted attention mostly in the context of distribution of flaws (Carpinteri, 1994; Carpinteri and Pugno, 2005) and of large scale yielding (Bazant and Chen, 1997; Brochard et al, 2015). In contrast, the combined temperature-loading rate-size scaling of the kinetic theory has attracted only little attention. Part of the difficulty stems to the logarithmic scaling which requires very large variations in loading rate and system size for proper investigation. Only the temperature scaling is easily achieved experimentally. In this respect, molecular simulations techniques offers an interesting alternative to experiments since one can easily vary the loading rate and the system size over orders of magnitudes. Slutsker (2005) propose a detailed study of Zhurkov's theory by molecular simulation but, to the best of our knowledge, the confrontation between strength and toughness scaling has not been studied so far. The purpose of this paper is to investigate with molecular simulation techniques the scalings of strength (tensile failure) and toughness (fracture failure) and confront the two scalings. We show, for a toy model (triangular lattice) and for graphene, that their failure is a thermally activated process exhibiting the expected Zhurkov-like scaling. Confronting strength and toughness, we highlight the essential difference in size scaling between fracture toughness and tensile strength. Thus, even though tensile failure and fracture failure arise both from the occurrence of a transition state, the distribution of these states differs radically. This study can serve as a starting point for the elaboration of a physically-based theory of initiation.

In section 2, we present the systems considered and the methodology used. In section 3, we present the results and we propose a theoretical analysis of the observed scaling in section 4.

2 Methods

We use molecular dynamics (MD) simulations to investigate failure at the atomistic scale. Molecular dynamics techniques give access to a space and time resolution hardly accessible experimentally. In particular, in this work, we focus on the scaling of the stress at failure with respect to temperature, system size and loading rate. Investigating such scaling requires to vary all those parameters over several orders of magnitude. Even though conventional MD is limited to millions of atoms simulated over nanoseconds, one can reasonably investigate 4 to 5 decades of scaling, which is enough for the present purpose.

We study two different materials: a toy model 2D solid and a realistic model of graphene. The respective
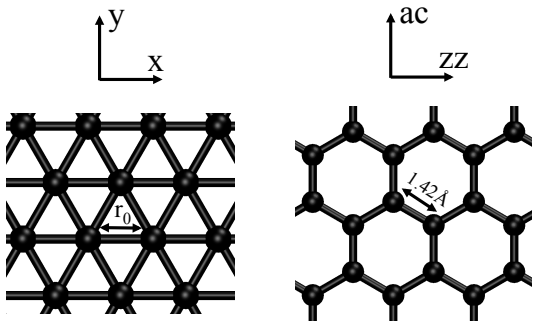
Fig. 1 Crystal structures of the toy model 2D solid (left) and of the graphene (right). The basis vectors give the name of the orientations used throughout this paper.

atomic structures of these two models are displayed in Figure 1. The toy model is a crystalline material made of a regular triangular lattice in which the inter-atomic potential is limited to harmonic interactions between nearest neighbors: $U = \sum_{i<j} U_{harmo}(r_{ij})$ with

$$U_{harmo}(r) = \begin{cases} \frac{K}{2}(r - r_0)^2 - U_{cr} & \text{if } r < r_{cr} \\ 0 & \text{otherwise} \end{cases} \quad (2)$$

where r_{ij} is the distance between atoms i and j, K, r_0 and $r_{cr} > r_0$ are the force constant, equilibrium distance and critical distance of the potential. The shift term $U_{cr} = \frac{K}{2}(r_{cr} - r_0)^2$ ensures continuity of the energy at $r = r_{cr}$. The potential is made irreversible, that is, once a bond is broken ($r > r_{cr}$) then it is removed from the system and can never reform even if the distance between the two atoms returns to less than r_{cr}. Doing so, we avoid any reversibility of the failure process (i.e., no 'healing' of bond).

The interest for such a toy model is that the results can be easily interpreted and confronted to theory. Toy models (including the triangular lattice) have been widely studied in the literature since the 1970's to understand the physics of failure. Thomson (1986) treated this type of toy model via Green's functions and, notably, identified energy barriers to failure similar to the expressions obtained in the present paper. Slepyan (2002) found analytical solutions for crack dynamics and considered in particular the triangular lattice. Many pursued these investigations in the following decades. Let us mention Marder and Gross (1994); Thomson et al (1992); Pechenik et al (2002) among others, who worked on the triangular lattice. To the best of our knowledge, the scaling study we report in this paper has never been done before.

For the triangular lattice we consider, the elastic mechanical behavior and tensile strength can be anticipated as follows, under small strain hypothesis at 0K:

elastic behavior: $\begin{cases} \sigma_{xx} = \sqrt{3}K\left(\frac{3\varepsilon_{xx}+\varepsilon_{yy}}{4}\right) \\ \sigma_{yy} = \sqrt{3}K\left(\frac{\varepsilon_{xx}+3\varepsilon_{yy}}{4}\right) \\ \sigma_{xy} = \frac{\sqrt{3}}{2}K\varepsilon_{xy} \end{cases}$ $\quad (3)$

tensile strength: $\begin{cases} \frac{\frac{\sigma_{yy}}{\sqrt{3}}+\sigma_{xy}}{K} \leq \frac{r_{cr}}{r_0} - 1 \\ \frac{\frac{\sigma_{yy}}{\sqrt{3}}-\sigma_{xy}}{K} \leq \frac{r_{cr}}{r_0} - 1 \\ \frac{3\sigma_{xx}-\sigma_{yy}}{2\sqrt{3}K} \leq \frac{r_{cr}}{r_0} - 1 \end{cases}$ $\quad (4)$

According to equations (3), one expects a simple linear elastic isotropic behavior with bulk modulus $\sqrt{3}K/2$ and shear modulus $\sqrt{3}K/4$. The tensile strength (Eq. 4), however, exhibits a non trivial surface. In particular, the strength is clearly anisotropic. The relations (2), (3) and (4) call for considering the following dimensionless quantities: $r^* = r/r_0$, $U^* = U/(Kr_0^2)$, $\sigma_-^* = \sigma_-/K$, $T^* = k_B T/(Kr_0^2)$ (k_B is Boltzmann constant). The results presented throughout this paper refer to those quantities.

The theoretical behavior given by Equations (3) and (4) assumes static equilibrium of the lattice which is the limit of low temperature (0K) and quasi-static loading. At finite temperatures and finite loading rate, thermal agitation and lattice vibrations (phonons) give rise to deviations from this theoretical prediction. In the following sections, we investigate those deviations. We perform MD simulations of periodic systems with $r_{cr}^* = 1.1$ and compute the tensile strength for various loading orientations, system sizes, temperatures and loading rates. More precisely, we consider 84 different loading orientations ranging from purely volumetric to purely deviatoric. We consider sizes ranging from $N = 30$ to $N = 491520$ atoms, temperatures from $T^* = 10^{-4}$ to $T^* = 1$, and loading rates from $\dot{\varepsilon}^* = 6.87 \cdot 10^{-11}$ to $\dot{\varepsilon}^* = 2.06 \cdot 10^{-5}$. Here, we define the dimensionless loading rate $\dot{\varepsilon}^* = \frac{d\varepsilon}{dt^*}$ with respect to the dimensionless time $t^* = t/\sqrt{K/m}$ where m is the mass of the atom. The Cauchy stress tensor is computed with the usual virial estimate (Allen and Tildesley, 1989). All these simulations are performed under isothermal conditions imposed by a Langevin thermostat and a velocity-Verlet integration scheme (Frenkel and Smit, 2002). In this work, we preferred to use a Langevin thermostat rather than the more conventional Nose-Hoover thermostat because the Nose-Hoover thermostat is known to be non-ergodic in the particular case of the harmonic oscillator (Legoll et al, 2007), which is an issue with respect to the toy model we study. Considering isothermal conditions is valid in this work because the system considered exhibit no irreversibilities untill the onset

of failure. In the general case, the temperature field is not uniform, for instance, plasticity at a crack tip induces a strong heating (Rice and Levy, 1969), which can dramatically affect the failure behavior (Zehnder and Rosakis, 1991; Flores and Dauskardt, 1999; Ponson et al, 2006; Wang et al, 2008).

Besides tensile failure, we also study the fracture failure of the toy model. One can estimate an approximate theoretical value of the toughness of the toy model by considering that fracture failure occurs when the first bond at a crack tip breaks. According to fracture mechanics, for a crack in the x direction and a loading in the y direction, the stress field is singular at the tip with an asymptotic stress ahead of the tip $\sigma_{yy}(r) \approx \frac{K_{Ic}}{\sqrt{2\pi r}}$, where r is the distance to the crack tip and K_{Ic} is the toughness. The first bond at tip breaks when the force it supports exceeds its carrying capacity. As a first approximation, one can estimate the stress it support by the integration of the stress singularity over the the length supported by the bond: $\int_0^{r_0/2} \sigma_{yy}(r) \, dr = K_{Ic}\sqrt{r_0/\pi}$ (for a crack in the x direction, the first bond is oblique and supports the load in y over a length $r_0/2$). The carrying capacity is given by the first two criteria in Equation (4) for the oblique bonds: $\frac{r_0}{2}\sqrt{3}K\left(\frac{r_{cr}}{r_0}-1\right)$. We thus obtain the following estimate of the toughness of the toy model:

$$K_{Ic} \sim K\sqrt{\frac{3\pi}{4}r_0}\left(\frac{r_{cr}}{r_0}-1\right) \tag{5}$$

Note that, unlike Equations (4) for strength, this is only an estimate that provides an order of magnitude. To study the fracture failure by molecular simulations, we simulate flawed systems with initial cracks initiated inside the material as displayed in Figure 2. A crack is initiated by removing bonds along a line. As for tensile failure, we consider periodic boundary conditions for the simulation of fracture failure. This choice is made to avoid spurious interface effects at non periodic boundaries. As a consequence, the cracked system is surrounded by periodic replica of the crack. The presence of a periodic crack has to be accounted for carefully in order to estimate the fracture toughness from the stress at failure. According to linear elastic fracture mechanics, when the system is submitted to a remote loading in the direction orthogonal to periodic cracks, the stress intensity K_I in mode I at the cracks' tips is :

$$K_I = \Sigma\sqrt{\pi a}C\left(\frac{2a}{L}, \frac{H}{L}\right) \tag{6}$$

where Σ is the average stress in the direction orthogonal to the crack, a is the half crack length and L and H are the x and y dimension of the periodic cell. One can identify the usual stress intensity for a finite crack in an infinite body ($\Sigma\sqrt{\pi a}$), and the coefficient $C\left(\frac{2a}{L}, \frac{H}{L}\right)$ is a correction due to the presence of periodic cracks. In particular, as $2a/L \to 0$, $C \to 1$ and one recovers the non-periodic case; and, as $2a/L \to 1$, $C \to +\infty$ since periodic cracks merge in this limit. There exists no analytic expression of $C\left(\frac{2a}{L}, \frac{H}{L}\right)$ but several numerical estimate have been proposed. In this work, we use the numerical estimate of Karihaloo et al (1996). According to fracture mechanics, failure occurs when the stress intensity reaches a critical value K_{Ic}, called toughness: Accordingly, the toughness and the average stress Σ_{cr} at failure are related according to:

$$\Sigma_{cr} = \frac{K_{Ic}}{\sqrt{\pi a}C\left(\frac{2a}{L}, \frac{H}{L}\right)} \tag{7}$$

Equation (7) can be used to estimate the toughness of the material from the result of a molecular simulation of the periodic system with initial crack. Note however, that Equation (7) is based on linear elastic fracture mechanics which assumes small scale yielding (Anderson (2005)). Therefore, it is valid only if the crack length and the distance between periodic replica is sufficiently large compared to the characteristic length $r_{pl} = \left(K_{Ic}/\sigma_{strength}\right)^2$ of the process zone at the crack tip. In practice, r_{pl} is often much larger than the size of an atom, and using Equation (7) at the atomic scale is questionable. We investigated this issue in previous work (Brochard et al, 2015, 2016). Regarding the present study, the toy model has a very low process zone: using the toughness estimation (Eq. 5), we obtain $r_{pl} = \pi r_0/4$. With the simplistic pair potential considered, fracture failure arises from a single bond breaking, that is r_{pl} is about the size of an atom. So we expect Equation (7) to be reproduced precisely at the atomic scale. In contrast, the characteristic length r_{pl} is about 1.5 nm for graphene and capturing the toughness with Equation (7) is possible for system at least 10 nm large which starts to be computationally expensive (see Brochard et al (2016)). So, we limit ourselves to the study of tensile failure for graphene.

We simulate fracture failure of the toy model for various system sizes, crack lengths, temperatures and loading rates. In all the simulations, cracks are initiated in the direction x and the systems are loaded in the y direction. Therefore, one obtains only the mode I toughness for crack propagation in the x direction. We consider crack lengths ranging from $2a/L = 0$ (i.e., tensile failure) to $2a/L = 1$ (i.e., fully separated). The range of system sizes and temperatures considered is the same as for tensile failure. Regarding loading rates,
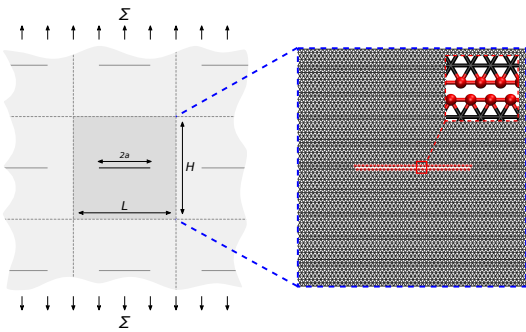
Fig. 2 System considered for the study of fracture failure: an initial crack is initiated by removing bonds along a line. Due to periodicity, the same crack exists in the periodic replica of the system.

Fig. 3 Type of system considered to investigate the scaling of toughness with the number of cracks: several periodic cracks are initiated within the elementary cell actually simulated. Periodic boundary conditions makes this geometry similar to that of Figure 2, but the two systems are not statistically equivalent; in particular, the corresponding toughnesses are different.

we consider rates one order of magnitude smaller than for tensile failure. Indeed, as will be discussed in section 4, excessive rates tend to introduce bias in our results and this bias appears more significant for the toughness estimate than for the strength estimate.

In addition to temperature, size and loading rate, we also investigate the scaling with respect to the number of initial crack in the periodic cell. To do so multiple cracks are initiated periodically in the system as displayed in Figure 3. The system being periodic, one recovers a situation similar to that of Figure 2. But the two situations are not statistically equivalent: in the original system (Fig. 2) all the periodic cracks experience an identical time evolution, whereas in the system of Figure 3 the time evolutions of the cracks in the primary cell are different. In particular, in the original system, failure occurs simultaneously at all the cracks, whereas in the system with multiple cracks, only one of the cracks in the primary cell fails. As a consequence, at same reduced crack length $2a/L$, temperature, system size and loading rate, the estimated toughness differs between the two systems. This points to a specific scaling with respect to the number of initial cracks in the periodic cell that we address together with the other factors. In the simulations, we consider a number of crack ranging from 1 to 256 (i.e., 16 by 16).

In addition to the toy model, we study the more realistic situation of graphene. Graphene is a crystalline material with honeycomb structure (Fig. 1) which has attracted a lot of attention because of its exceptional physical properties. Graphene failure has been the focus of many studies in the literature (see, for instance, the review of Zhang et al (2015) and references therein). It appears that graphene is brittle, i.e., exhibits high strength ($\sim$ 130 GPa) but relatively low toughness ($\sim$ 4 MPa.$\sqrt{m}$). Many molecular simulation studies (Omeltchenko et al (1997); Belytschko et al (2002); Khare et al (2007); Zhang et al (2012); Moura and Marder (2013); De-
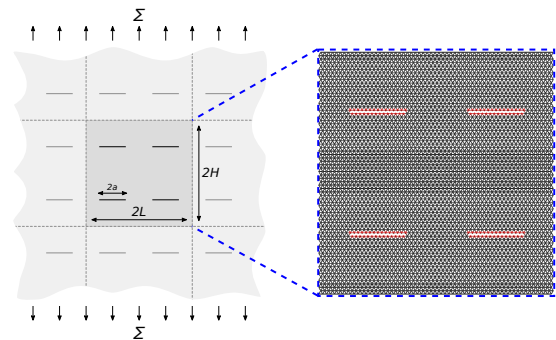
wapriya et al (2014) to mention a few) investigated the failure properties of graphene from its tolerance to flaw to the effects of polycrystalinity. In the present paper, we consider graphene as a realistic case study in contrast with the case of the toy model.

Several inter-atomic potentials exist to simulate graphene. We consider the REBO potential of Brenner (1990). This potential is known to lead to an excessive strength due a spurious bump in the aromatic carbon-carbon interaction force as the material is stretched (Shenderova et al, 2000; Belytschko et al, 2002). A way to circumvent this problem consists in modifying the switching function performing a smooth cut-off of the C-C interaction between $r_{min} = 1.7$Å and $r_{max} = 2.0$Å. The distance r_{min} is set to 2.0Å so that the function performs a sharp cut-off of the energy at 2.0Å (Yazdani and Hatami, 2015). This modification effectively suppresses the bump and leads to an elasticity and strength that compares well with ab-initio calculations (Liu et al, 2007) and experimental measurements (Lee et al, 2008). Note, however, that this modification introduces a discontinuity in the original formulation of the energy which must be handled carefully. In the present work, all the implementation of the molecular dynamics rely on the atomic forces only and the associated energy potential is the continuous integration of the force field. The general methodology is the same as for the simulation of the toy model except that we investigate tensile strength only. The graphene systems studied contain 2508 to 2618 atoms (about 8×8 nm^2) and are loaded with a strain rate of 0.001 ps^{-1} at temperatures ranging from 0K to 2700K. Even though graphene has a two dimensional structure, the failure behavior is affected by the third dimension. To investigate this question we perform both simulations in 3D and simulations in 2D by constraining the material in the plane.
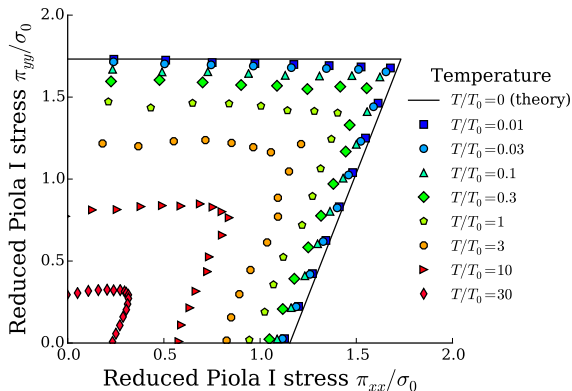
Fig. 4 Tensile strength obtained for the toy model for various temperatures and loading directions. No shear is applied to the material so that $\sigma_{xy} = 0$ for all the points represented.

Fig. 5 Tensile strength results for graphene simulated in 2D (results in 3D are similar). All points are in the plane $\sigma_{xy} = 0$. The results at 0K are obtained by minimization (static equilibrium) and not by molecular dynamics.

All the calculations are performed with LAMMPS software (http://lammps.sandia.gov, (Plimpton, 1995)).

3 Results

In this section we present the results of the molecular simulations. A detailed analysis of the scalings is presented in section 4.

3.1 Effect of temperature on strength

First of all, we focus on the effect of temperature on tensile strength. We show in Figure 4 the failure surface of the toy model at various temperatures. For sake of generality, the displayed results are reduced with respect to the characteristic tensile strength $\sigma_0^* = \sigma_0/K = r_{cr}^* - 1$. Moreover, the temperature scale is given relative to the characteristic failure temperature $T_0^* = \frac{k_B T_0}{K r_0^2} = (r_{cr}^* - 1)^2$. At 0K, the theoretical failure surface is given by Equations (4). This theoretical surface is drawn with a black line in Figure 4. Note that we display the Piola I stresses (first Piola-Kirchhoff stress) and not the Cauchy stresses as is usually done. The reason is that the theoretical failure surface of Equations (4) is calculated for the undeformed configuration, whereas the Cauchy stress relates to the deformed configuration. In order to confront the results of molecular simulation to the 0K theory, we convert the Cauchy stress tensor ($\underline{\underline{\sigma}}$) into the Piola I stress tensor ($\underline{\underline{\pi}}$) as follows:

$$\underline{\underline{\pi}} = \det\left(\underline{\underline{F}}\right) \underline{\underline{\sigma}}^t \cdot \underline{\underline{F}}^{-t} \tag{8}$$

where $\underline{F}$ is the deformation gradient tensor. In the limit of small strains, the Piola I stresses are almost equal to

the Cauchy stresses. But, for the case of the toy model, the deformations are of the order of $r_{cr}^* - 1 = 10\%$ which is large enough to induce significant differences between the two tensors. In terms of Piola I stresses, the simulations results at low temperatures are in very good agreement with the 0K theory.

One can readily interpret the shape of the tensile failure surface. It exhibits two modes of failure. The horizontal branch (π_{yy} constant) corresponds to the failure of the bonds at $\pm 30°$ of the y axis in the crystal structure (Fig. 1). The oblique branch ($3\pi_{xx} - \pi_{yy}$ constant) corresponds to the failure of the bonds along the x axis in the crystal structure. As temperature is increased, one observes a decrease of the tensile strength. Interestingly, this decrease appears almost independent of the loading direction.

In Figure 5, we display the tensile failure surface of graphene for various temperatures. As for the toy model, we represent the Piola stress which differs significantly from the Cauchy stress since the deformations reach $\sim 20\%$ at failure. Again, the tensile strength decreases with temperature. However, this decrease is no more independent of the loading direction: the strength decreases faster in the zigzag ('zz') direction than in the armchair ('ac') direction. Therefore, the orientational invariance observed for the toy model is a peculiarity of this system. One can clearly identify two regimes in the tensile failure surface of graphene: an horizontal branch (π_{ac} almost constant) corresponding to the failure of the bonds oriented in the armchair direction in the crystal structure (Fig. 1); and a vertical branch (π_{zz} almost constant) corresponding to the failure of the bonds at $\pm 30°$ of the zigzag direction in the crystal structure. Of course, this bond failure interpretation is an idealization since the actual atomic interactions in

Fig. 6 Failure stress of the pre-cracked systems in function of the initial crack length $2a/L$ at various temperatures. The marks are the simulation results, whereas the lines are the fits with fracture mechanics (Eq. 7) providing estimations of the toughness. For clarity, the curves are arbitrarily shifted v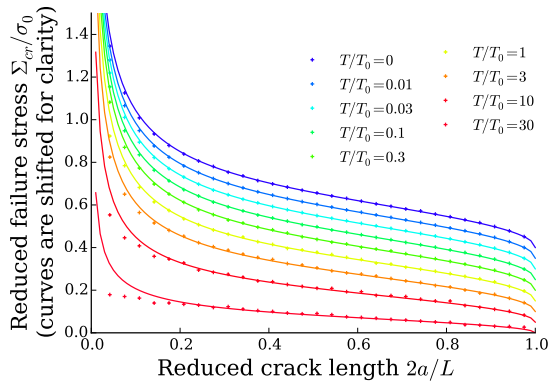ertically. In an exact representation, all the curves converge at 0 for $2a/L = 1$. The 0K case is obtained by energy minimization and not by molecular dynamics.

Fig. 7 Scaling of strength and toughness of the toy model with temperature. The error bars for strength correspond to the standard deviation associated to the loading direction. The error bars for the toughness correspond to the standard deviation associated to the initial crack length.

graphene are many-body and much more complex than bond interactions.

3.2 Effect of temperature on toughness

In this section, we focus on the toughness estimation. We perform molecular simulations of pre-cracked systems as illustrated in Figure 2. When changing the initial crack length, one expects Equation (7) of fracture mechanics to apply, thus providing a way to estimate the toughness. We perform simulations at different temperatures and we display the stress at failure in function of the initial crack length in Figure 6. Then, we fit each curve with Equation (7) to derive the evolution of the toughness with the temperature. For sake of clarity, the results of Figure 6 are shifted vertically. In an actual representation, all curves would end at 0 for $2a/L = 1$.

Fits with the theory of fracture mechanics are precise, except at the largest temperatures were deviations are observed for small crack lengths. At 0K, we obtain a toughness $K_{Ic}^* = \frac{K_{Ic}}{K\sqrt{r_0}} = 0.198$. This value compares well with the theoretical estimate (Eq. 5): $K_{Ic}^* = \sqrt{3\pi/4}\,(r_{cr}^* - 1) = 0.153$. The tensile strength in the same loading direction (y) at 0K is given by Eq. 4: $\sigma_{strength}^* = \frac{\sigma_{strength}}{K} = \sqrt{3}\,(r_{cr}^* - 1) = 0.1\sqrt{3}$. Therefore the characteristic length of the process zone at 0K is $r_{pl}^* = \frac{r_{pl}}{r_0} \approx 1.31$. As expected, the process zone is about the size of an atom, and fracture mechanics is expected to capture well the failure behavior even at the atomic scale. This is indeed observed in Figure 6. Nevertheless, at high temperature ($T/T_0 = 30$), the same calculation gives a much larger process zone: $r_{pl}^* = 4.69$.

Hence the deviation from fracture mechanics at high temperatures.

With this method, we can estimate the evolution of the toughness with temperature. The next section confront the temperature scalings of strength and toughness.

3.3 Trends with temperature

We compare in Figure 7 the scalings of strength and toughness with temperature. The error bars have different meanings for the two quantities. For strength, it represent the standard deviation between the various loading directions (Fig. 4), whereas, for the toughness, it represents the standard deviation associated to the estimations from equation (7) at the various values of $2a/L$. In particular, the error bars for toughness increases with the temperature because of the discrepancy discussed in the previous section. In the following of the paper, all errors bars refer to these definitions.

As temperature is increased, both strength and toughness decrease. Interestingly, the toughness decreases less rapidly than the strength. The ratio between toughness and strength is also the size of the process zone ($r_{pl} = (K_{Ic}/\sigma_{strength})^2$) which, therefore, increases significantly. Apart from this difference, strength and toughness exhibit very similar scalings. We draw empirical scaling laws in Figure 7 (dashed lines) which depends on the square root of temperature:

$$\frac{\sigma_{strength}}{\sigma_{strength}\,(0K)} \text{ or } \frac{K_{Ic}}{K_{Ic}\,(0K)} = 1 - \sqrt{\alpha T} \qquad (9)$$

α is the single fitting parameter and takes a different value for strength and toughness. It is notable that
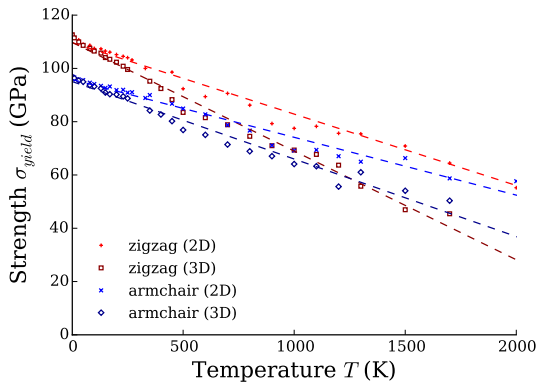
Fig. 8 Scaling of graphene strength with temperature. The strength in the armchair (ac) and zigzag (zz) directions are plotted separately. We also present results for the graphene simulated in 3D and for graphene constrained in 2D. The dashed lines are trend lines.

the same expression captures both strength and toughness trends. It appears that this scaling is not linear as predicted by Zhurkov's theory (Eq. 1), but we show in the following section that this scaling law is consistent with Zhurkov's approach.

Likewise, we display in Figure 8 the scaling of graphene strength with temperature. In contrast with the toy model, the decrease of strength depends on the orientation. So we distinguish the evolution for the armchair direction to that for the zigzag direction. We also distinguish the results for graphene constrained in 2D to that in 3D. We observe that strength decreases almost linearly with temperature, in both directions and irrespective of 2D constraint, as expected from Zhurkov's theory. The difference of scaling with the toy model shows that the scaling with temperature is closely related to the nature of the atomic interactions. Since the linear scaling is common in real materials, one can suspect that some aspects of the toy model are unrealistic. We discuss this point later on. The strength of graphene decreases more rapidly in 3D than in 2D. This is expected since constraining the material in 2D prevents transition paths to failure that would involve out-of-plane deformations of the atomic structure. The energy barrier to failure is expected to be larger in 2D than in 3D, hence the difference in temperature scaling.

3.4 Effect of loading rate and system size

According to the theory of thermally activated processes, the scaling of failure should combine temperature, loading rate and system size. Following Equation (1) with N_{TS} degenerate transition states, the failure stress is expected to be a function of $T \ln \left(\frac{N_{TS}}{\dot{\varepsilon}/\varepsilon_{cr}} \right)$, with

$\dot{\varepsilon_{cr}}$ a constant of the dimension of a strain rate. One expects that this rate-temperature-size equivalence is characterized by a single master curve. So we completed the toy model scaling by performing a large series of simulations to investigate the effect of system size and loading rate, for both fracture failure and tensile failure. The results are displayed in Figure 9 for tensile failure and in Figure 10 for fracture failure.

We observe that both strength and toughness increase with the loading rate. However, while strength decreases with the number of atoms, the toughness appears almost independent of it. Our interpretation is that the number N_{TS} of transition states scales with the number of atoms in a flawless material, and with the number of cracks in the case of a cracked material. Accordingly, we investigated the scaling with the number of cracks as explained in the methods (section 2). Doing so, we observe a decrease of the toughness with the number of initial cracks.

In Figure 9, we observe that all the strengths align very well on a single master curve validating the rate-temperature-size equivalence with the number of atoms as a proxy for the number of transition states. On the top chart, all the simulations are performed at the same temperature ($T^* = T_0^* = (r_{cr}^* - 1)^2$). A few results corresponding to large systems submitted to high loading rates deviates from the master curve. We attribute this discrepancy to insufficient equilibration that prevents sampling correctly the phase space of atomic configurations. On the bottom chart, all the simulations are performed with the same number of atoms ($N = 270$) and the strengths relative to 0K are plotted in function of the quantity $\ln \left(\frac{N}{\dot{\varepsilon}/\varepsilon_{cr}} \right) \frac{T}{T_0}$. By fitting appropriately the constant $\dot{\varepsilon_{cr}}$, the data points align very well along a master curve.

In Figure 10, we observe that the toughness results also align along a single master curve considering the number of cracks as a proxy for the number of transition states. The chart on top represents the toughness relative to 0K for systems simulated at the temperature $T^* = T_0^*$. As for strength, we observe a deviation of the molecular simulation results from the scaling law at high loading rates, and the deviation increases with the system size. The deviation is more pronounced than for strength: for a system of given size, reaching the scaling law requires to consider loading rates about two orders of magnitude smaller than for the strength simulations. As before, we attribute this deviation to an insufficient equilibration which introduces a bias in the sampling of the phase space. Interestingly, cracked bodies seem to require much more time to equilibrate than flawless systems. The bottom chart in Figure 10 displays the results for systems of identical sizes with 1 crack
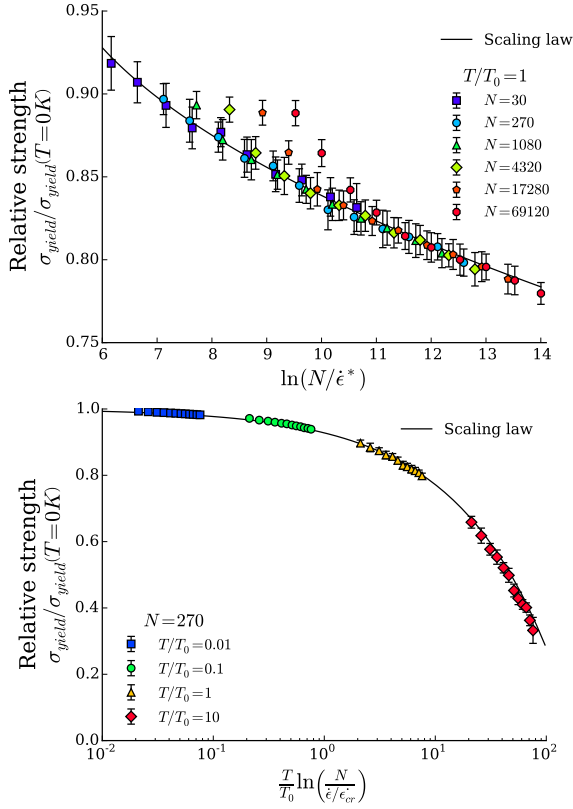
Fig. 9 Scaling of the strength of the toy model with respect to the combination of system size, temperature and loading rate. The top chart displays the results of systems all at temperature $T^* = T_0^* = (r_{cr}^* - 1)^2$ but of various sizes and loading rates. The strength relative to 0K is plotted in function of the quantity $\ln(N/\dot{\varepsilon}^*)$. The bottom chart displays the results of systems all of the same size ($N = 270$) but at various temperatures and loading rates. The strength relative to 0K is plotted in function of the quantity $\ln\left(\frac{N}{\dot{\varepsilon}/\varepsilon_{cr}}\right)\frac{T}{T_0}$. In both chart, the results align very well on a general master curve which is accurately fitted by the proposed scaling law (Eq. 12).

Fig. 10 Scaling of the toughness of the toy model with respect to the combination of number of cracks, temperature and loading rate. The top chart displays the results for systems simulated at $T^* = T_0^*$ with various number of cracks N_{crack} and loading rates $\dot{\varepsilon}$. We plot the toughness relative to 0K in function of the quantity $\ln\left(\frac{N_{crack}}{\dot{\varepsilon}^*}\right)$. The bottom chart for systems with $N_{crack} = 1$ at various temperatures and loading rates. We plot the toughness relative to 0K in function of the quantity $\ln\left(\frac{N_{crack}}{\dot{\varepsilon}/\varepsilon_{cr}}\right)\frac{T}{T_0}$. In both chart, the results exhibit the scaling behavior which is well captured by the proposed scaling law (Eq. 12).

at various temperatures and loading rates. We plot the toughness relative to 0K in function of the quantity $\ln\left(\frac{N_{crack}}{\dot{\varepsilon}/\varepsilon_{cr}}\right)\frac{T}{T_0}$. Here also, with an appropriate choice of the constant $\dot{\varepsilon}_{cr}$, the results align well along a master curve. And, again, the results of systems submitted to the highest loading rate deviate from the scaling law.

4 Analysis and discussion

One can interpret the observed scaling by adopting a statistical physics description akin to Zhurkov's theory. We develop such an analysis in this section.

4.1 Toy model scaling

We consider failure as a thermally activated process with no reverse process. Following Boltzmann statistics, the probability of occurrence of a transition state leading to failure is proportional to $\exp\left(-\frac{\Delta E_{TS}}{k_B T}\right)$, where $\Delta E_{TS} > 0$ is the energy barrier that has to be overcome. In the toy model, failure occurs when one of the bonds has a length exceeding the critical distance r_{cr}. At 0K, all atoms are in static equilibrium and failure occurs precisely at the theoretical surface (Eq. 4). At finite temperature though, failure can occur below this limit because of thermal agitation. Let us consider the material loaded below the theoretical surface (Eq. 4). The ground state (state of minimum energy) at this loading is the system at 0K. A transition states leading to fail-

ure is such that one of the bonds reaches $r = r_{cr}$. Since all bonds are harmonic, the energy barrier to reach the transition state is quadratic[1]:

$$\Delta E_{TS} = \frac{K}{2}\kappa\left(r_{cr} - r\right)^2 \tag{10}$$

with $\kappa > 0$ a constant. This energy barrier can be rewritten in term of stress by taking advantage of the linearity of the mechanical behavior: the length of a bond depends linearly on the strain and stress. We have:

$$\Delta E_{TS} = k_B T_{cr} \left(1 - \frac{\sigma_{failure}}{\sigma_{failure}\left(0K\right)}\right)^2 \tag{11}$$

where $k_B T_{cr} = \frac{K}{2}\kappa\left(r_{cr} - r_0\right)^2 = \frac{\kappa}{2}k_B T_0$ is a characteristic temperature of failure. Expression 11 is valid for both tensile failure and fracture failure. A difference appears regarding the number of transitions states. For tensile failure, by periodicity of the atomic structure, the number of transition states is proportional to the number of atoms. For fracture failure, it is proportional to the number of cracks. Therefore, the probability of failure which is the cumulative probability of all the degenerate transition states takes the form $\propto N_{TS}\exp\left(-\frac{\Delta E_{TS}}{k_B T}\right)$, with $N_{TS} = N$ for tensile failure and $N_{TS} = N_{crack}$ for fracture failure. This Boltzmann statistics can also be interpreted as the inverse of the characteristic time of recurrence of this event during a time evolution. Equivalently, the probability of failure over a given time scale is inversely proportional to the loading rate. We finally obtain the scaling relation:

$$\frac{\sigma_{failure}}{\sigma_{failure}\left(0K\right)} = 1 - \sqrt{\ln\left(\frac{N_{TS}}{\dot{\varepsilon}/\dot{\varepsilon_{cr}}}\right)\frac{T}{T_{cr}}} \tag{12}$$

where $\dot{\varepsilon_{cr}}$ is a constant which has the inverse dimension of a time. The ratio $\frac{\sigma_{failure}}{\sigma_{failure}\left(0K\right)}$ is the ratio of strength for tensile failure and the ratio of toughness for fracture failure. This scaling law is precisely of the form of the empirical law we suggested in the previous section (Eq. 9). In Figures 9 and 10, we display the best fit of the master curve with Equation (12) (for strength : $T_{cr}^* = \frac{k_B T_{cr}}{K r_0^2} = 1.923$ and $\ln\left(\dot{\varepsilon_{cr}}^*\right) = \ln\left(\dot{\varepsilon_{cr}}\sqrt{K/m}\right) = 5.0$, for toughness : $T_{cr}^* = 1.923$ and $\ln\left(\dot{\varepsilon_{cr}}^*\right) = 4.3$). This scaling law captures well all the results for the toy model.

---

[1] ΔE_{TS} is the integration of the repelling force to exert on the atoms of the failing bond to bring it to failure, while maintaining all other atoms at static equilibrium. By linearity of the bond network, this repelling force depends linearly on the bond length, hence the quadratic energy barrier.
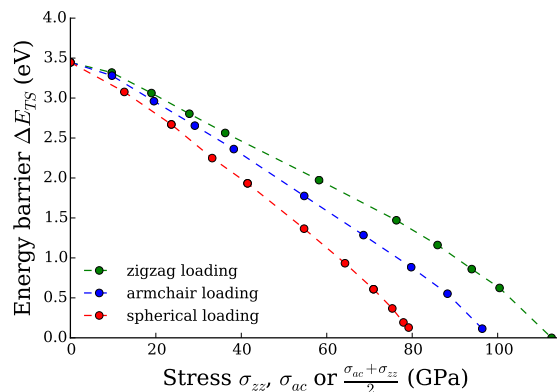
Fig. 11 Energy barrier to reach the transition state for graphene failing in the armchair direction. The linear trend suggests a relation $\Delta E_{TS} \propto -\left(\sigma - \sigma_{strength}\left(0K\right)\right)$, hence a strength scaling $\frac{\sigma_{strength}}{\sigma_{strength}\left(0K\right)} = 1 - \ln\left(\frac{N_{TS}}{\dot{\varepsilon}/\dot{\varepsilon_{cr}}}\right)\frac{T}{T_{cr}}$ consistent with the results of Figure 8.

4.2 Graphene scaling

In the previous section, we derived a scaling law for the toy model in which the failure depends on the square root of temperature. This scaling differs markedly from the linear scaling we obtained for graphene and which is commonly observed for real materials (Eq. 1). This difference is a direct consequence of the peculiar expression of the energy barrier for the toy model (Eq. 11). This expression holds for perfectly harmonic atomic interactions (Eq. 2). This idealized potential is convenient for theoretical derivations such as that of the scaling law, but it exhibits a discontinuity in its derivative at the critical length r_{cr} which, of course, is not representative of real atomic interactions. Instead, significant non linearity is expected in the atomic interactions when approaching failure. This is indeed the case for graphene simulated with the REBO potential. How this difference impacts the energy barrier ΔE_{TS} is hard to anticipate since a formal demonstration is no more possible. Nevertheless, one can estimate numerically ΔE_{TS} by searching for the minimum transition path between an initial configuration (intact material) and a final configuration (broken material).

We can estimate numerically the energy barrier for graphene failure. The minimum transition path is found by increasing the length of a bond while relaxing all other degrees of freedom. We display in Figure 11 the energy barrier in function of the stress for different loading directions (armchair, zigzag and spherical). The x-intercept corresponds to the failure at 0K ($\sigma_{failure}\left(0K\right)$). The trend is clearly different from the energy barrier of the toy model (Eq. 11). Instead the energy barrier depends almost linearly on the stress, that is:

$$\Delta E_{TS} = k_B T_{cr} \left(1 - \frac{\sigma_{failure}}{\sigma_{failure}(0K)} \right) \qquad (13)$$

with T_{cr} the temperature corresponding to the energy barrier at zero stress. Combining this expression with the statistics for thermally activated process, one recovers a linear scaling law for failure, consistent with the results of Figure 8:

$$\frac{\sigma_{failure}}{\sigma_{failure}(0K)} = 1 - \ln\left(\frac{N_{TS}}{\dot{\varepsilon}/\dot{\varepsilon}_{cr}} \right) \frac{T}{T_{cr}} \qquad (14)$$

This linear scaling is expected to be more relevant for real materials than that obtained for the toy model (Eq. 12) since a linear scaling with temperature is commonly observed experimentally (Zhurkov, 1984).

5 Conclusion

The analysis of scaling provides a general rate-temperature-size equivalence for both tensile failure and fracture failure. The main difference between strength and toughness stems to the number of transitions states N_{TS} which scales with the number of atoms for tensile failure and with the number of cracks for fracture failure. Failure always originates from the occurrence of a transition state, but the distribution of transition states and the associated energy barriers is strongly affected by stress concentration and the presence of flaws. Tensile failure can occur at any location in the material, fracture failure is limited to a small number of transition states at the crack tip.

There are several important implications to this study:

– The rate-temperature-size equivalence relates the failure properties under very different conditions. One can easily relate failure at the atomistic level, typically $\sim 10^3 - 10^6$ atoms loaded at $\sim 10^{10} - 10^7 s^{-1}$, and at the macroscopic level, typically $\sim 10^{23}$ atoms loaded at rate $\sim 1 s^{-1}$. Proper confrontation of failure properties at different scales can be achieved by taking advantage of the rate-temperature-size equivalence.

– Knowing the effect of temperature on failure is enough to predict the scaling with loading rate and system size. This is of practical interest, in particular for molecular simulation studies, in which it is easy to vary temperature with little or no additional computational cost; whereas increasing the system size or decreasing the loading rate over orders of magnitudes comes with very significant computational costs, if not prohibitive.

– Stress concentration at a crack tip strongly localizes the transition states. The transition from fracture failure to tensile failure through flaws of more moderate stress concentrations (e.g., notch, holes etc.) involves the transition from a regime of very few possible transition states, to a regime of lots of transition states. How the number of transition states and their energy barrier depends on the stress concentration is thus an important question in the formalization of a theory of failure initiation.

The scaling law we propose here is not directly applicable to the prediction of failure of real materials since one would have to account for the presence of existing flaws of various length and density. Extending the type of scaling laws we propose to distribution of flaws is a perspective.

References

Allen MP, Tildesley DJ (1989) Computer simulation of liquids. Oxford University Press

Anderson TL (2005) Fracture Mechanics: Fundamentals and Applications. CRC Press, Taylor & Francis Group

Argon A (1979) Plastic deformation in metallic glasses. Acta Metallurgica 27(1):47–58, DOI 10.1016/0001-6160(79)90055-5, URL http://linkinghub.elsevier.com/retrieve/pii/0001616079900555

Bazant ZP, Chen EP (1997) Scaling of Structural Failure. Applied Mechanics Reviews 50(10):593, DOI 10.1115/1.3101672, URL http://appliedmechanicsreviews.asmedigitalcollection.asme.org/art

Belytschko T, Xiao SP, Schatz GC, Ruoff RS (2002) Atomistic simulations of nanotube fracture. Physical Review B 65(23):235,430, DOI 10.1103/PhysRevB.65.235430, URL http://link.aps.org/doi/10.1103/PhysRevB.65.235430

Brenner DW (1990) Empirical potential for hydrocarbons for use in simulating the chemical vapor deposition of diamond films. Physical Review B 42(15):9458–9471, DOI 10.1103/PhysRevB.46.1948.2, URL http://link.aps.org/doi/10.1103/PhysRevB.42.9458

Brochard L, Hantal G, Laubie H, Ulm FJ, Pellenq RJM (2015) Capturing material toughness by molecular simulation: accounting for large yielding effects and limits. International Journal of Frac-

ture 194(2):149–167, DOI 10.1007/s10704-015-0045-y, URL http://link.springer.com/10.1007/s10704-015-0045-y

Brochard L, Tejada IG, Sab K (2016) From yield to fracture, failure initiation captured by molecular simulation. Journal of the Mechanics and Physics of Solids 95:632–646, DOI 10.1016/j.jmps.2016.05.005, URL http://www.sciencedirect.com/science/article/pii/S0022509616300424 http://linkinghub.elsevier.com/retrieve/pii/S0022509616300424

Carpinteri A (1994) Scaling laws and renormalization groups for strength and toughness of disordered materials. International Journal of Solids and Structures 31(3):291–302, DOI 10.1016/0020-7683(94)90107-4, URL http://linkinghub.elsevier.com/retrieve/pii/0020768394901074

Carpinteri A, Pugno N (2005) Are scaling laws on strength of solids related to mechanics or to geometry? Nature Materials 4(6):421–423, DOI 10.1038/nmat1408, URL http://www.nature.com/doifinder/10.1038/nmat1408

Dewapriya MAN, Rajapakse RKND, Phani AS (2014) Atomistic and continuum modelling of temperature-dependent fracture of graphene. International Journal of Fracture 187(2):199–212, DOI 10.1007/s10704-014-9931-y, URL http://link.springer.com/10.1007/s10704-014-9931-y

Dugdale D (1960) Yielding of steel sheets containing slits. Journal of the Mechanics and Physics of Solids 8(2):100–104, DOI 10.1016/0022-5096(60)90013-2

Dumitrica T, Hua M, Yakobson BI (2006) Symmetry-, time-, and temperature-dependent strength of carbon nanotubes. Proceedings of the National Academy of Sciences 103(16):6105–6109, DOI 10.1073/pnas.0600945103, URL http://www.pnas.org/cgi/doi/10.1073/pnas.0600945103

Flores KM, Dauskardt RH (1999) Enhanced toughness due to stable crack tip damage zones in bulk metallic glass. Scripta Materialia 41(9):937–943, DOI 10.1016/S1359-6462(99)00243-2, URL http://linkinghub.elsevier.com/retrieve/pii/S1359646299002432

Frenkel D, Smit B (2002) Undestanding Molecular Simulation: From Algorithms to Applications, 2nd edn. Academic Press

Johnson WL, Samwer K (2005) A Universal Criterion for Plastic Yielding of Metallic Glasses with a (T/Tg)ˆ(2/3) Temperature Dependence. Physical Review Letters 95(19):195,501, DOI 10.1103/PhysRevLett.95.195501, URL https://link.aps.org/doi/10.1103/PhysRevLett.95.195501

Karihaloo BL, Wang J, Grzybowski M (1996) Doubly periodic arrays of bridged cracks and short fibre-reinforced cementitious composites. Journal of the Mechanics and Physics of Solids 44(10):1565–1586, DOI 10.1016/0022-5096(96)00053-1, URL http://linkinghub.elsevier.com/retrieve/pii/0022509696000531

Khare R, Mielke SL, Paci JT, Zhang S, Ballarini R, Schatz GC, Belytschko T (2007) Coupled quantum mechanical/molecular mechanical modeling of the fracture of defective carbon nanotubes and graphene sheets. Physical Review B 75(7):075,412, DOI 10.1103/PhysRevB.75.075412, URL https://link.aps.org/doi/10.1103/PhysRevB.75.075412

Lee C, Wei X, Kysar JW, Hone J (2008) Measurement of the Elastic Properties and Intrinsic Strength of Monolayer Graphene. Science 321(5887):385–388, DOI 10.1126/science.1157996, URL http://www.ncbi.nlm.nih.gov/pubmed/18635798 http://www.sciencemag.org/cgi/doi/10.1126/science.1157996, 47749150628

Legoll F, Luskin M, Moeckel R (2007) Non-Ergodicity of the NoséHoover Thermostatted Harmonic Oscillator. Archive for Rational Mechanics and Analysis 184(3):449–463, DOI 10.1007/s00205-006-0029-1, URL http://link.springer.com/10.1007/s00205-006-0029-1

Leguillon D (2002) Strength or toughness? A criterion for crack onset at a notch. European Journal of Mechanics, A/Solids 21(1):61–72, DOI 10.1016/S0997-7538(01)01184-6

Liu F, Ming P, Li J (2007) Ab initio calculation of ideal strength and phonon instability of graphene under tension. Physical Review B 76(6):064,120, DOI 10.1103/PhysRevB.76.064120, URL http://link.aps.org/doi/10.1103/PhysRevB.76.064120

Marder M, Gross S (1994) Origin of Crack Tip Instabilities. Journal of the Mechanics and Physics of Solids 43(1):1–48, DOI 10.1016/0022-5096(94)00060-I, URL http://arxiv.org/abs/chao-dyn/9410009, 9410009

Moura MJB, Marder M (2013) Tearing of free-standing graphene. Physical Review E 88(3):032,405, DOI 10.1103/PhysRevE.88.032405, URL http://link.aps.org/doi/10.1103/PhysRevE.88.032405

Novozhilov V (1969) On a necessary and sufficient criterion for brittle strength. Journal of Applied Mathematics and Mechanics 33(2):201–210, DOI 10.1016/0021-8928(69)90025-2, URL http://linkinghub.elsevier.com/retrieve/pii/0021892869900252

Omeltchenko A, Yu J, Kalia RK, Vashishta P (1997) Crack Front Propagation and Fracture in a Graphite Sheet: A Molecular-Dynamics Study on Parallel Computers. Physical Review Letters 78(11):2148–2151, DOI 10.1103/PhysRevLett.78.2148, URL https://link.aps.org/doi/10.1103/PhysRevLett.78.2148

Pechenik L, Levine H, Kessler Da (2002) Steady-state mode I cracks in a viscoelastic triangular lattice.

Journal of the Mechanics and Physics of Solids 50(3):583–613, DOI 10.1016/S0022-5096(01)00061-8, URL http://arxiv.org/abs/cond-mat/0002314 http://linkinghub.elsevier.com/retrieve/pii/S0022509601000618 0002314

Petrov VA, Orlov AN (1975) Contribution of thermal fluctuations to the scattering and the gauge effect of longevity. International Journal of Fracture 11(5):881–886, DOI 10.1007/BF00012904, URL http://link.springer.com/10.1007/BF00012904

Petrov VA, Orlov AN (1976) Statistical kinetics of thermally activated fracture. International Journal of Fracture 12(2):231–238, DOI 10.1007/BF00036980, URL http://link.springer.com/10.1007/BF00036980

Plimpton S (1995) Fast Parallel Algorithms for Short-Range Molecular Dynamics. Journal of Computational Physics 117(1):1–19, DOI 10.1006/jcph.1995.1039, URL http://linkinghub.elsevier.com/retrieve/pii/S002199918571039X

Ponson L, Bonamy D, Barbier L (2006) Cleaved surface of ¡math display="inline"¿ ¡mrow¿ ¡mi¿i¡/mi¿ ¡mtext¿¡/mtext¿ ¡mi mathvariant="normal"¿Al¡/mi¿ ¡mi mathvariant="normal"¿Pd¡/mi¿ ¡mi mathvariant="normal"¿Mn¡/mi¿ ¡/mrow¿ ¡/math¿ quasicrystals: Influence of the local temperature elevation at. Physical Review B 74(18):184,205, DOI 10.1103/PhysRevB.74.184205, URL https://link.aps.org/doi/10.1103/PhysRevB.74.184205

Regel' VR, Slutsker AI, Tomashevski ÉE (1972) The kinetic nature of the strength of solids. Soviet Physics Uspekhi 15(1):45–65, DOI 10.1070/PU1972v015n01ABEH004945, URL http://stacks.iop.org/0038-5670/15/i=1/a=R03?key=crossref.123f17f2adf8d374f849d4039738ff14

Rice JR, Levy N (1969) Local Heating by Plastic Deformation at a Crack Tip. Physics of Strength and Plasticity pp 277–293

Schuh C, Hufnagel T, Ramamurty U (2007) Mechanical behavior of amorphous alloys. Acta Materialia 55(12):4067–4109, DOI 10.1016/j.actamat.2007.01.052, URL http://linkinghub.elsevier.com/retrieve/pii/S1359645407000122X

Shenderova Oa, Brenner DW, Omeltchenko a, Su X, Yang LH (2000) Atomistic modeling of the fracture of polycrystalline diamond. Physical Review B 61(6):3877–3888, DOI 10.1103/PhysRevB.61.3877, URL http://link.aps.org/doi/10.1103/PhysRevB.61.3877\nhttp/

Slepyan LI (2002) Models and Phenomena in Fracture Mechanics. Foundations of Engineering Mechanics, Springer Berlin Heidelberg, Berlin, Heidelberg, DOI 10.1007/978-3-540-48010-5, URL

http://link.springer.com/10.1007/978-3-540-48010-5

Slutsker AI (2005) Atomic-Level Fluctuation Mechanism of the Fracture of Solids (Computer Simulation Studies). Physics of the Solid State 47(5):801, DOI 10.1134/1.1924836, URL http://link.springer.com/10.1134/1.1924836

Thomson R (1986) Physics of Fracture. In: Ehrenreich H, Turnbull D (eds) Solid state physics, vol 39, Academic Press, pp 1–129, DOI 10.1016/S0081-1947(08)60368-9, URL http://linkinghub.elsevier.com/retrieve/pii/S0081194708603689

Thomson R, Zhou SJ, Carlsson AE, Tewary VK (1992) Lattice imperfections studied by use of lattice Greens functions. Physical Review B 46(17):10,613–10,622, DOI 10.1103/PhysRevB.46.10613, URL https://link.aps.org/doi/10.1103/PhysRevB.46.10613

Wang G, Chan K, Xu X, Wang W (2008) Instability of crack propagation in brittle bulk metallic glass. Acta Materialia 56(19):5845–5860, DOI 10.1016/j.actamat.2008.08.005, URL http://dx.doi.org/10.1016/j.actamat.2008.08.005 http://linkinghub.elsevier.com/retrieve/pii/S1359645408005636

Wei C, Cho K, Srivastava D (2003) Tensile strength of carbon nanotubes under realistic temperature and strain rate. Physical Review B 67(11):115,407, DOI 10.1103/PhysRevB.67.115407, URL http://arxiv.org/abs/cond-mat/0202513 https://link.aps.org/doi/10.1103/PhysRevB.67.115407, 0202513

Yazdani H, Hatami K (2015) Failure criterion for graphene in biaxial loadinga molecular dynamics study. Modelling and Simulation in Materials Science and Engineering 23(6):065,004, DOI 10.1088/0965-0393/23/6/065004, URL http://stacks.iop.org/0965-0393/23/i=6/a=065004?key=crossref.66817f771850338a194c2b825

Zehnder AT, Rosakis AJ (1991) On the temperature distribution at the vicinity of dynamically propagating cracks in 4340 steel. Journal of the Mechanics and Physics of Solids 39(3):385–415, DOI 10.1016/0022-5096(91)90019-K, URL http://linkinghub.elsevier.com/retrieve/pii/002250969190019K

Zhang T, Li X, Kadkhodaei S, Gao H (2012) Flaw insensitive fracture in nanocrystalline graphene. Nano Letters 12(9):4605–4610, DOI 10.1021/nl301908b

Zhang T, Li X, Gao H (2015) Fracture of graphene: a review. International Journal of Fracture 196(1-2):1–31, DOI 10.1007/s10704-015-0039-9, URL http://link.springer.com/10.1007/s10704-015-0039-9

Zhu T, Li J, Samanta A, Leach A, Gall K (2008) Temperature and Strain-Rate Dependence of Surface Dislocation Nucleation. Physical Review Letters 100(2):025,502, DOI 10.1103/PhysRevLett.100.025502, URL

https://link.aps.org/doi/10.1103/PhysRevLett.100.025502

Zhurkov SN (1984) Kinetic concept of the strength of solids. International Journal of Fracture 26(4):295–307, DOI 10.1007/BF00962961, URL http://link.springer.com/10.1007/BF00962961